Infinite Science
Publishing

Original Research Article

Rapid prototyping of a four terminal fringing field electrical impedance spectroscopy sensor

P. Kleinschnittger[1]*, G. Baghdasaryan[1], A. Bahr[1,2], and W. Krautschneider[1]

[1] *Institute of Integrated Circuits, Hamburg University of Technology, Hamburg, Germany*
[2] *Sensor System Electronics, Institute of Electrical Engineering and Information Technology, Kiel University, Kiel, Germany*
* *Corresponding author, email: patrick.kleinschnittger@tuhh.de*

Abstract: The ability of a tumor cell to metastasize, influenced by the specific cell junctions between tumor cells, is important in the mortality of cancer patients. To evaluate the electric properties of cell junctions Electrical Impedance Spectroscopy (EIS), a promising tool to analyze the cell-specific, frequency-dependent impedance of cancer cells, can be used to perform measurements during the confluent growth of the metastatic cells on the surface of a sensor. This paper aims to develop a prototype for a comb-structured, planar fringing field sensor (FFS) that can be used with four terminal (4T) EIS cell measurements. Due to the novelty of this 4T sensor, no exact design criteria are defined in literature. A rapid prototyping approach, utilizing a novel silver ink, which can be used with a desktop inkjet printer, and a material jetting printer, are used to quickly explore the design space. Design parameters for the 4T FFS are derived based on known relationships from two terminal electrodes and experimental results. Analyzing ion solution measurements of the different FFS designs, we were able to show that the relationship between the width of the digit and the gap in-between as well as the number of digits are influencing the performance of the FFS, resulting in an optimized design. With this design we were able to show the performance improvement a 4T sensor has over a 2T sensor and differentiate significantly between different ion solutions. Although desktop silver inkjet printing still has some limitations, it is a promising approach to rapidly prototype biosensors. Overall, we were able to define design parameters for optimizing the fringing field sensor performance.

I. Introduction

Cancer is a heterogeneous group of diseases characterized by an uncontrolled growth of abnormal cells in the body. It is a widespread disease and in Germany the second most common cause of death with a lifetime mortality rate of about 20 % for women and 25 % for men [1]. The ability of a tumor to metastasize, i.e. to spread to other parts of the body and form secondary tumors there, is a decisive factor in the mortality of cancer patients [2]. The process of metastasis is still poorly understood, but it is proven that the specific cell junctions between cancer cells play an important role in the ability of a tumor to metastasize [3].

One way to analyze the different cell junction properties of normal and metastatic cells is to determine the electrical properties of the connection and the cell. Here, Electrical Impedance Spectroscopy (EIS) is a promising tool. It allows the user to examine biological tissue non-

invasively, radiation-free and without affecting the composition of the material under test (MUT). It can be used to identify the specific tissue anatomy and to diagnose its pathological status [4]–[7]. Especially in the field of tumor diagnosis EIS is a promising method of identifying cancer [6] or differentiating between benign and malignant tumor cells [5]. In some medical disciplines it is already the standard in clinical use, e.g. in the field of melanoma screening [7]. In all cases, the distinction between healthy and cancerous tissue is made via the cell-specific, frequency-dependent impedance. Here, a frequency-variable voltage or current signal is applied to the sample and the system response (current strength or voltage) is measured. The impedance is then calculated as the ratio between voltage and current signal and analyzed over the whole frequency spectrum. It is therefore directly dependent on the conductivity and relative permittivity of the MUT. Working with biological cells an increase in

frequency leads to a decrease in the relative permittivity and an increase in the conductivity, resulting in three different dispersion phases (α-, β- and γ-dispersion) [4]. For the characterization of tumor cells especially the α-dispersion and the β-dispersion are relevant, because in this phases the direct influence of the cells electric properties and the differences in the membrane capacitance can be seen [4], [5]. An experimental setup of the conventional two terminal (2T) EIS configuration, consisting of a working and counter electrode opposing each other and surrounding the MUT is shown in Figure 1a.

EIS can be used to analyze the electric properties of cell junctions between metastatic cancer cells by performing measurements during the cell adhesion and proliferation phase. For this, a setup can be used where the cells are grown on the surface of a planar sensor so that the electromagnetic fields are mainly expanding into these cells and the measured impedance spectrum is mainly defined by the properties of the thin tissue layer and not the surrounding nutrient solution. Therefore, a planar fringing field sensor (FFS) needs to be developed. By placing the electrodes in a planar configuration the characteristic fringing field distribution occurs compared to the uniform field distribution between working and counter electrode in the conventional two chamber (Figure 1) [8], [9]. The working principle of these sensors is explained in detail in [8], [9].
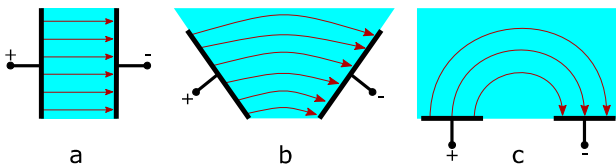

Figure 1: Visualization of the production of a four terminal fringing field sensor: from (a) a conventionally two terminal EIS-measurement chamber whose (b) electrodes opened up and moved (c) to the planar plane to provide a fringing field with one-sided access to the MUT. The figure is adapted from Mamishev et al., 2004. The working and counter electrodes are black, the electric field is red and the MUT is turquoise.

Important for the sensor is its capability to measure the impedance artifact-free over a broad frequency spectrum to detect the behavior of the cells during α- and β-dispersion. This poses a particular challenge for conventional two terminal measurement systems, because the frequency dependent electrolytic double layer (DL) affects the measurements. The DL is formed by the interaction of water molecule dipoles and ions with the surface of an electrode resulting in a high capacitance in the low frequency range influencing the impedance significantly [4]. The influence of the DL capacitance can be avoided by a four terminal measurement system, which is described in detail in [4], [5]. Unfortunately, such a planar sensor does not exist on the market, since only two terminal interdigitated electrodes (IDE) are available.

Therefore, the goal of this paper is to develop a prototype for four terminal EIS FFS, which can be used for planar cell measurements. To achieve this goal, the conventional four terminal (4T) EIS configuration must be transferred to the planar plane (Figure 2). Since there are only design criteria for a two terminal IDE in literature, a rapid prototyping approach is used, to quickly explore the design space experimentally and adapt the design to the measurement results. For an easier and faster result different ion solutions instead of cell measurements are used and the sensor is analyzed according to later on defined quality criteria. According to the rapid prototyping approach, the production times of the different FFS designs should be minimized. That means a fast but precise production method with a high resolution, which can be used in house, to reduce order and delivery times, is necessary. Additionally, the sensors need to be corrosion- and water-resistant, as well as highly conductive. Since cell experiments are to be carried out with the sensors later on, cell death caused by the material must be prevented. For this purpose, the sensors must be made of a biocompatible material. For this reason, inkjet printing with conductive silver ink is chosen to manufacture the electrodes, which fulfills these requirements [10]. Using a novel silver ink the complete printing process can be performed with a standard desktop printer, making it possible to realize a fast production process of a prototype, taking only approx. 30 minutes from the design changes to the first measurement. For the development of the measurement chamber a material jetting printer is used.
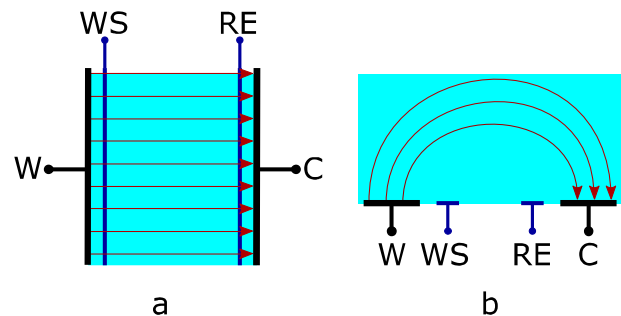

Figure 2: Visualization of two different 4T EIS measurement systems. In (a) the conventional EIS and in (b) the planar configuration are shown. The working (W) and counter electrodes (C) are black, the working sense (WS) and reference electrode (RE) are blue, the electric field is red and the MUT is turquoise.

II. Material and methods
In this paper, the FFSs are fabricated using an Epson EcoTank ET-M1170 monochromatic inkjet printer (Epson, Suwa, Japan). They are printed using NovaCentrix Metalon JS-ADEV ET010 silver inkjet ink (Novacentrix, Austin, USA), an experimental, electrically conductive ink, consisting of 40 % silver nano particles with an average size of 32 nm, 10-15 % ethylene glycol and 0.2-1 % polyethylene glycol 4-(tert-octylphenyl) ether [11].

Melinex ST506 (DuPont Teijin Film, Dumfries, United Kingdom), a heat stabilized polyester film pretreated for better ink adhesion was used as a printing substrate. The material properties of the ink and the substrate are listed in Table 1.

Table 1: Material properties of the nano silver ink and the substrate material

Mechanical Properties	Unit	Value
JS-ADEV ET010		
Specific gravity (calc.)		1.43
Surface tension	Dyne/cm	24.2
Viscosity	cP (at 25 °C)	3.6
Sheet resistance	Ohm/square	0.26
Volume resistivity (cure time 15 min at 120 °C)	Ohm*m	8E-5
Melinex ST506		
Dielectric Constant		2.9
Dielectric Strength	Volts/mil	3000
Surface Resistivity	Ohm/sq	1E13
Volume Resistivity	Ohm*m	1E15
Shrinkage MD (150 °C)	%	0.15
Shrinkage TD (150 °C)	%	0.15

Before printing a FFS, the substrate was electrostatically discharged to reduce the smudging during printing, using a grounded electrode. The design files were converted to a pdf file and transmitted to the printer. After printing, the FFS is cured at 120° C for 15 minutes to improve the conductivity and the adherence of the silver ink to the substrate.

The measurement chamber is fabricated using the Keyence AGILISTA-3200W 3D printer (Keyence Deutschland GmbH, Neu-Ilsenburg, Germany), a high-resolution material jetting printer. AR-H1 (Keyence Deutschland GmbH, Neu-Ilsenburg, Germany) a firm polyurethane material in combination with the AR-S1 (Keyence Deutschland GmbH, Neu-Ilsenburg, Germany) support material was used as a printing material.

II.I. Design

For the design of the FFSs a comb structure with four conducting paths, representing the working, working sense, reference and counter electrode is used. An exemplary design can be seen in Figure 3. The green line defines the border between the connection part to the measuring system and the submerged sensory part of the FFS.

There are no information to be found in literature about designing four terminal planar electrodes. Therefore, since the comb structure is similar to commercial two terminal IDEs, it is assumed that the design rules for two terminal IDEs can be applied in this case as well. Designing a planar sensor is always an iterative process with different trade-offs between the electrode properties like the penetration depth (PD), the measurement sensitivity (MS), the dynamic range and signal strength. While the dynamic range and the signal strength are not directly dependent on the geometry of the electrode, the MS and PD are dependent and therefore, need to be considered when designing the FFS. The MS describes the ratio of the change with the sensor output in regards to the change of the physical output value and is largely influenced by the area of the sensor [9], [12]. The PD describes the distance in z-direction until which the electric fields penetrate the material under test. It is influenced by the spatial wavelength of the IDE (λ), which is defined as the distance between the digits of same polarity [8]. Therefore the PD is directly dependent on width of a digit w and the distance in between d described in (1) [8], [13].

$$PD \cong 0.5 * \lambda = w + d \qquad (1)$$

While we want to keep the MS high, to recognize small deviations in the MUT, we want the PD as low as possible to not over penetrate the MUT, i.e. there needs to be a tradeoff between increasing w to increase MS and decreasing w to decrease PD. In addition, for an electrode design with $N > 2$, the cross coupling between the different electric fields, which is increasing with lower distance between the digits d, has to be considered [12].
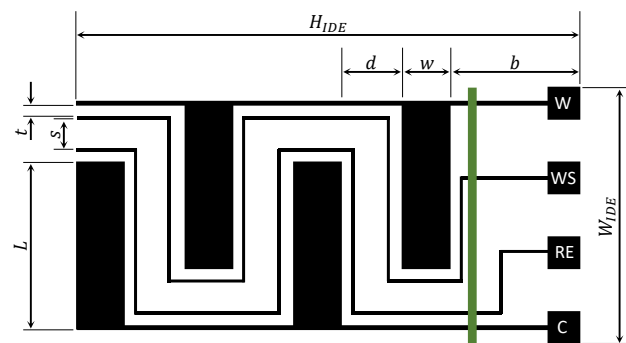

Figure 3: Exemplary design of the 4T FFS with the working (W), working sense (WS), reference (RE) and counter (C) electrode. On the left side of the green line is the measurement part and on the right side the connection part to the sensory system of the FFS. The dimensioning parameters are shown.

For applications in biological media, optimization methods for the geometric parameters can be found in the literature [14], [15]. Although the original optimization objective, to reduce the influence of the double layer effect on the electrode, is in this design approach not required, since a 4T electrode is used, the resulting optimization rules are applied in this design as well to increase the sensitivity of the FFS. Ibrahim et al. showed, that there is an ideal ratio

a between the width of the digits w and the gap d, as described in (2), as well as an influence of the number of digits on the sensitivity of the measurement [14].

$$a = \frac{d}{w} = 0.66 \qquad (2)$$

To design the FFSs, the area of the sensor, given in (3), was kept constant at $A = 622,7 \ mm^2$ to minimize its impact on the MS. To use the FFS with the developed measurement chamber $b = 16 \ mm$, $H_{IDE} = 76 \ mm$ and the size of the connectors for the measurement system had to be kept constant as well. For an easier design, the width of the working sense and reference electrode was kept at the lowest printable width of 0.25 mm, since studies showed that a significantly smaller working sense and reference electrode in comparison to the working and counter electrode increase the sensitivity [16]. The distance s between the working sense and reference electrode was kept at 2 mm. The exception here is the design D_{81} were s is only 1 mm due to printing limitations. Both electrodes are placed equidistant from the working and counter electrode. The width of the part of the working and counter electrode, which is not part of the digits, was kept at 1 mm. The thickness of the ink layer is 3 µm.

$$A = N * L * w \qquad (3)$$

In order to validate whether the ideal ratio a from Ibrahim et al. also applies in the four-terminal application, d and w were chosen according to (2). For comparison the counterexample with $a = 1.5$ was also designed. Three different numbers of digits, $N = 4, 6$ and 8 were chosen. The FFS designs are labelled as D_{xy}, where the subscript $x = N$ and y describes the d/w ratio with $y = 1$ for $a = 0.67$ and $y = 2$ for $a = 1.5$. Due to limitations in the resolution of the printing process, the distance t could not be reduced further without smearing of the printed traces, therefore higher digit numbers could not be realized. In total six different designs were evaluated. The parameters of each design can be seen in Table 2.

Table 2: Design parameters of the six FFS designs. All values are given in mm

	W_{IDE}	L	w	d	s	t	PD
D_{41}	24.23	15.57	10	6.67	2	2.58	10.67
D_{42}	34.64	22.05	7.06	10.59	2	4.56	17.65
D_{61}	22.43	16.14	6.43	4.29	2	1.39	10.72
D_{62}	32.02	23.35	4.44	6.67	2	2.59	11.11
D_{81}	21.59	16.43	4.47	3.16	1	1.33	7.9
D_{82}	30.86	24	3.24	4.86	2	1.68	8.1

In order to carry out the EIS measurements a suitable measurement chamber was designed and 3D printed. The

chamber consists of a container where the measurements are performed and a support structure to allow a for a good connection between the FFS and the measurement system. The container has a fill depth of 20 mm, a fill width of 37.5 mm and a fill height of 66 mm. The support structure has a width of 37.5 mm and a height of 15 mm. A thin slit with a depth of 0.65 mm is placed in front of the support structure though which the sensor is inserted. To ensure that the sensor does not bend, it is mounted in a 0.5 mm deep groove at the bottom of the chamber. To easily fill and empty the chamber with ion solution as well as to keep the liquid lost through evaporation low the container has a T-shape opening at the upper cover. The schematic of the measurement chamber with the resulting dimensions can be seen in Figure 4.
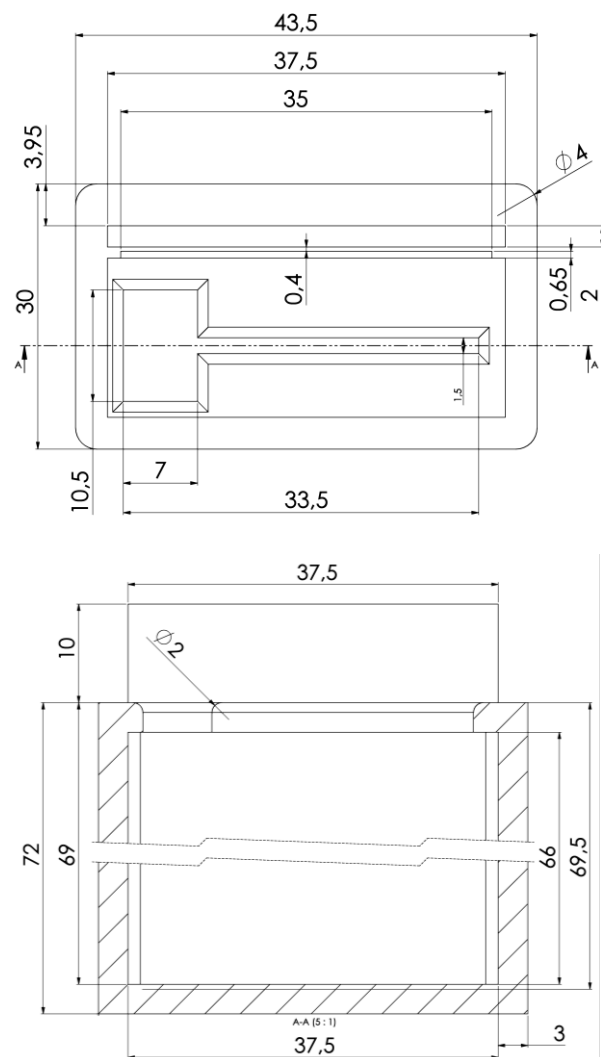

*Figure 4: CAD-Design schematic of the measurement chamber*

II.II. Experimental Validation of the FFSs

Each FFS-design was characterized using a 0.1 mol/l sodium chloride (NaCl) solution. With the most suitable design, comparative experiments with potassium (KCl), magnesium ($MgCl_2$), calcium chloride ($CaCl_2$) and a mixture of 50 % NaCl and 50 % KCl solution, representative of the most important free-moving ions in

the human body [17], were carried out. Moreover, a comparison between the four-terminal design developed here and a two terminal design with the same geometric parameters was performed. Three Electrodes were printed for each design and measurements were repeated five times per electrode, resulting in 15 total measurements per FFS design. For each measurement 49 ml ion solution was used. A 14 mV amplitude AC voltage was applied and the frequency was varied between 1 Hz to 1 MHz. Experiments were performed using the potentiostat Interface 1000E (Gamry Instruments Inc., Warminster Township, USA), a precise two-, three- and four terminal potentiostat. Equipment cables are shielded against electromagnetic interference and calibration was carried out before the measurements. The measurement setup including the FFS is shown as a photograph and a wiring schematic in Fig. 5.

III. Results and discussion

In order to analyze the different designs and characterize the most optimal design for this application, four quality criteria were defined. Firstly, the smoothness of the magnitude as well as the phase curve, because the ideal curve should show a frequency independence with a phase value of zero and a response as flat as possible, since a four terminal setup to avoid the parasitic DL effects and a well conducting NaCl-solution were used for the experiments. In order to parameterize this criterion, the normalized difference of the impedance magnitude and phase values from their respective average values over the entire frequency range is calculated and averaged over the frequency spectrum, giving the parameters Mag_{diff} and $Phase_{diff}$.
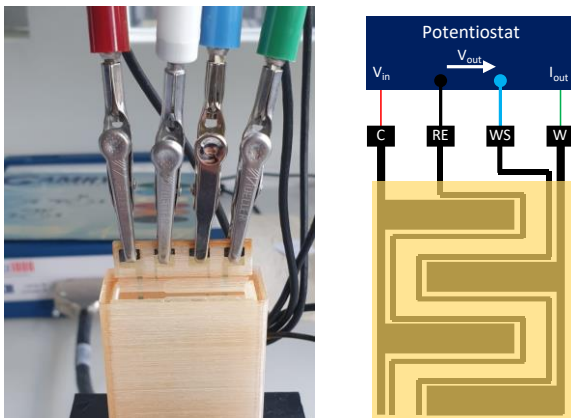
a: Photograph of the setup   b: wiring schematic

Figure 5: Experimental Setup for the ion solution measurements. In a) the measurement setup with the final FFS inside the measurement chamber is shown. In b) the wiring schematic including the ion solution (yellow). In both figures the counter electrode (C) is red, the reference electrode (RE) is in a white and in b black, the working sense electrode (WS) is blue and the working electrode (W) is green. In the background of a) the Gamry Interface 1000E potentiostat can be seen.

The second quality criterion is a reliable reproducibility of the measured values, represented by a low scattering of the values in the whole frequency range. It is also a measure of the MS, since a low scattering increases the probability to differentiate between MUTs, which show a similar impedance spectrum. This criterion can be parameterized by the average standard deviation STD_M and STD_P. The third quality criterion is a low phase value, given by the averaged phase value $Phase_m$, as the ion solution theoretically behaves like an ideal resistance. The last quality criterion is a low PD.

In Fig. 6 the Bode plots, for all six FFSs designs are depicted with their respective error bars representing the standard deviation. As one can see, all plots deviate from the expected ideal case, showing a slight phase increase in the low frequency range (1 Hz to 1000 Hz) and an increase of the phase as well as a scattering of the measurement values in the high frequency range (above 300 kHz).

The deviation in the low frequency range can be explained by a low remaining influence of the DL. As stated in literature, it is hard to totally avoid the parasitic influence of the DL capacitance as it is strongly dependent on several experimental and instrumentation parameters [4]. With planar electrode setup the effects of the DL cannot be fully compensated, because, due to opening up the regular electrode arrangement to obtain a fringing field, the position of the working sense and reference electrode is changed and not covering the whole height of the electric field anymore, as shown in Figure 2. Due to a maximum phase that is more than twice as high, it can be seen that the FFS designs D_{61}, D_{81} and D_{82} are significantly more influenced by the DL capacitance compared to the other designs. Since the experimental conditions as well as the sensor area is constant between all the experiments, the digit number N seems to influence the susceptibility of a sensor to the DL capacitance. However, this does not explain the difference between D_{61} and D_{62}, since they both have the same number of digits. Comparing all designs, it can be seen by the phase maximum that, with the exception of the designs D_{61} and D_{62}, the designs with the non-ideal a-ratio have a higher susceptibility to the DL effect than those with an a-ratio of 0.66.

A possible explanation for the higher phase maximum of the theoretically better design can be the lower t parameter, resulting in a stronger cross coupling of the electric fields. Presumably, this cross coupling then seems to influence the susceptibility for the DL capacitance. This would lead to the assumption that there is an optimal distance t between the working and working sense electrode, where the susceptibility for the DL capacitance and the parasitic effects of the interaction between working sense and reference electrode, which were discovered by Barth et al., 2019, are in an equilibrium. To validate this theory a simulation of the measurements needs to be performed in a future work. Overall, it seems that the a-ratio as design criterion, which was developed by Ibrahim et al., 2013 for

the theoretical simulation of a two-terminal system, is transferable to a real application with a four-terminal system.

The phase increase of the measurement values in the high frequency range above 300 kHz is due to the parasitic geometric capacitance, which is not part of the MUT response [5]. The scattering of the impedance at 1 MHz is due internal measurement system of the Gamry potentiostat.

To compare the designs, the quality criterion parameters for each FFS where normalized and weighted. Since the scattering is essential for the later differentiation of ionic solutions as well as for the reproducibility, it is weighted with a factor of three. To represent the parasitic influence the DL capacitance, the frequency dependent change of the impedances and the mean phase are weighted with a factor of two. In this design space exploration, the PD is not as decisive and therefore weighted with a factor of one. The mean average phase value is weighted with a factor of one. Since the aim is to minimize the parameters of the quality criteria, a lower value is better. The results are shown in Table 3.
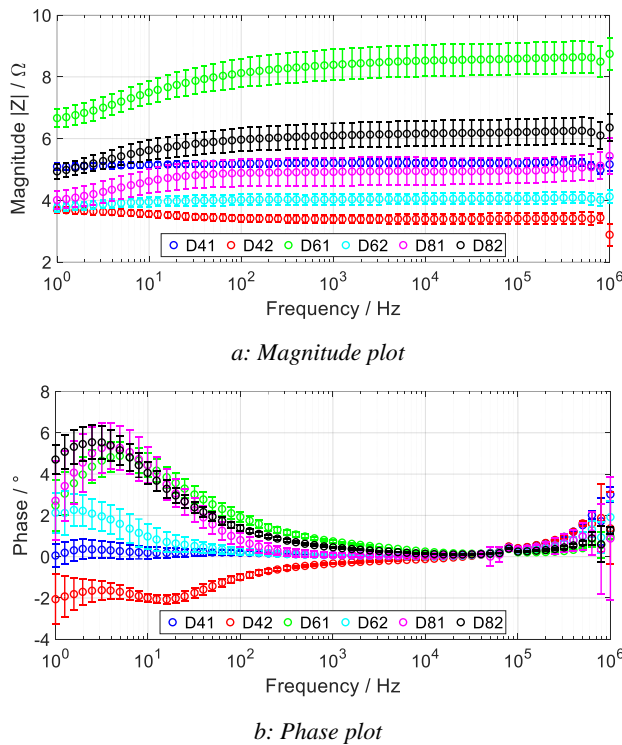

a: Magnitude plot

b: Phase plot

Figure 6: Bode plot with error bars of the six FFS designs, a shows the magnitude and b the phase plot. The x-axis is in logarithmic scale.

It can be seen by comparing D_{61}, D_{81} and D_{82} to the other designs, that the standard deviation of the measurements increases as the number of digits increases (STD_M increase of 126 % for D_{62} to D_{82} and 20 % for D_{42} to D_{62}) and the factor d decreases (STD_M increase of 173 % for D_{61} to D_{62} and 10 % for D_{81} to D_{82}). The reason for this, as already noted in the literature [12], could be the increase in cross

coupling between the electrical fields of the individual fingers, due to a smaller distance between the digits.

Table 3: Normed and weighted quality criterion parameters

	D_{41}	D_{42}	D_{61}	D_{62}	D_{81}	D_{82}
STD_P	0.28	0.41	0.47	0.47	0.97	0.40
STD_M	0.19	0.25	0.83	0.30	0.75	0.68
$Phase_{diff}$	0.15	0.28	0.43	0.18	0.50	0.47
Mag_{diff}	0.07	0.14	0.84	0.10	0.36	0.49
$Phase_m$	0.06	0.09	0.27	0.10	0.23	0.27
PD	0.23	0.24	0.15	0.15	0.11	0.11
SUM	0.98	1.41	2.97	1.31	2.92	2.42

Overall, it can be seen, that the FFS design D_{41} performs the best in nearly every quality criterion. Exception here is the PD, which in this case is not as important as in further applications, since enough ion solution was used to secure the total coverage of the PD. Therefore, D_{41} is the most promising FFS prototype. For further experiments with cell monolayers the PD needs to be drastically decreased.

III.II. Differentiating between ion solutions

Figure 7 shows the magnitude and phase plot for the differentiation of different ion solutions using FFS design D_{41}. It is evident looking at the error bars of the magnitude plot, that the sensor is capable to significantly differentiate between the five different ion solutions.

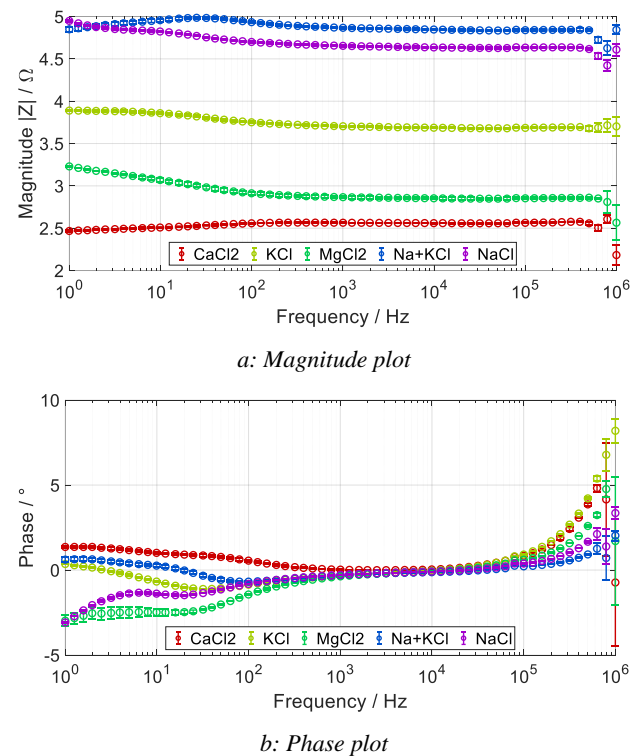*a: Magnitude plot*

b: Phase plot

Figure 7: Bode plot with error bars for the different Ion solutions, (a) shows the magnitude and (b) the phase plot. Measurements were performed using the D41 FFS design. The x-axis is in logarithmic scale.

Moreover, it is possible to differentiate between the pure NaCl and the mixed solution, indicating a sufficient MS. Interesting to see is, that the mixed Na+KCl solution has a higher impedance than the NaCl- or the KCl-solution. This can be explained, by the concentration-dependent conductivity of an electrolyte solution, were the individual concentration of two different cations is halved [18]. A more detailed explanation would exceed the scope of this paper, but can be found in Hamann et al., 2005.

III.III. Comparison between 2T and 4T

Although, as explained above, the DL has a small influence on the measurements in the low frequency range up to 1000 Hz, the newly developed four terminal FFS design D_{41} allows a measurement of the MUT with negligible influence of the DL, as illustrated in Figure 8. For this measurement the working and working sense as well as the counter and the reference electrode from the sensor were shorted, showing the influence of the DL capacitance on the two-terminal measurement. The influence of the DL capacitance decreases with increasing frequency, as it is described in literature [4] and can be seen in the phase plot. At approx. 1 kHz the curve of the graphs are similar, showing the cutoff frequency of the DL capacitance. This reinforces the statement, that the deviation of the phase for the designs D_{61}, D_{81} and D_{82} in the low frequency range in Fig. 6bis caused by the DL capacitance.
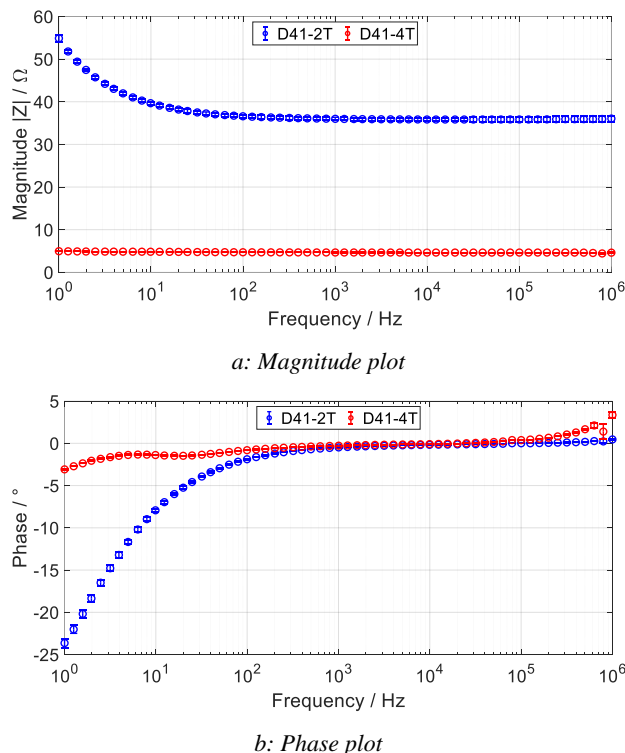

a: Magnitude plot

b: Phase plot

Figure 8: Bode plot with error bars comparing the two-terminal setup with the four terminal setup, a shows the magnitude and b the phase plot. Measurements were performed using the D_{41} FFS design. The x-axis is in logarithmic scale.

III.IV. Limitations of the printing process

Using the experimental ink JS-ADEV ET010 some limitations in the printing process were identified. Foremost the printer used needle wheels inside to move the printing substrate. These needle wheels caused smearing on the printed electrode and needed to be removed, causing some minor mechanical changes to the printer. In addition, the electrostatic discharging had to be done carefully, otherwise causing smearing as well. The smallest structure printable with a sufficient quality was at 0.25 mm.

Whereas printing small gaps next to small structures is feasible below 1 mm, printing small gaps next to big structures, i.e. the digits of the FFS, is difficult, due to smearing. The reason for this is according to the manufacturer a missing binder in the ink. The binder had to be removed in this ink variant, since it has caused clogging of the printer head in previous iterations. The manufacturer told us, that in the next iteration a new binder will be added, to increase the adhesion on the substrate and reduce smearing, allowing then for smaller structures and gaps.

IV. Conclusions

This work presents the successful fabrication of a four terminal FFS prototype, usable for 4T EIS measurements. The sensor is capable to differentiate between different ion solutions, including a mixture of potassium and sodium. Although there are still a few limitations due to the ink, conductive inkjet printing is a promising rapid prototyping approach for the produced biosensors. Since with the next iteration of the silver ink smaller structures and gaps are feasible, smaller PDs will be achievable and therefore moving the presented prototype to a usable state for cell monolayer measurements.

In summary, this work shows a promising new fabrication approach for the fringing-field sensors and provides the proof that the produced sensors are stable enough to be used for four terminal electrical impedance spectroscopy. Moreover, the design parameters for optimizing the sensor performance have been identified and a set of ideal parameters is given. For future research, a Finite Element Method simulation of the FFS should be performed to validate the theory of the optimum distance t between the working and working sense, as well as the counter and reference electrode.

AUTHOR'S STATEMENT
Authors state no conflict of interest. Informed consent has been obtained from all individuals included in this study.

REFERENCES

[1] B. Barnes *et al.*, "Krebs in Deutschland für 2017/2018," 2021. [Online].Available: https://www.krebsdaten.de/Krebs/DE/Content/Publikationen/Krebs_in_Deutschland/krebs_in_deutschland_inhalt.html.

[2] H. Dillekås, M. S. Rogers, and O. Straume, "Are 90% of deaths from cancer caused by metastases?," *Cancer Med.*, vol. 8, no. 12, pp. 5574–5576, Sep. 2019, doi: 10.1002/cam4.2474.

[3] D. Kyuno, A. Takasawa, S. Kikuchi, I. Takemasa, M. Osanai, and T. Kojima, "Role of tight junctions in the epithelial-to-mesenchymal transition of cancer cells," *Biochim. Biophys. Acta - Biomembr.*, vol. 1863, no. 3, p. 183503, Mar. 2021, doi: 10.1016/j.bbamem.2020.183503.

[4] V. F. Lvovich, *Impedance Spectroscopy*, 1. Hoboken, NJ, USA: John Wiley & Sons, Inc., 2012.

[5] V. S. Teixeira, T. Barth, V. Labitzky, U. Schumacher, and W. Krautschneider, "Electrical Impedance Spectroscopy for Characterization of Prostate PC-3 and DU 145 Cancer Cells," in *2019 41st Annual International Conference of the IEEE Engineering in Medicine and Biology Society (EMBC)*, Jul. 2019, pp. 6485–6489, doi: 10.1109/EMBC.2019.8856627.

[6] D. Haemmerich, S. T. Staelin, J. Z. Tsai, S. Tungjitkusolmun, D. M. Mahvi, and J. G. Webster, "In vivo electrical conductivity of hepatic tumours," *Physiol. Meas.*, vol. 24, no. 2, pp. 251–260, May 2003, doi: 10.1088/0967-3334/24/2/302.

[7] P. Åberg, U. Birgersson, P. Elsner, P. Mohr, and S. Ollmar, "Electrical impedance spectroscopy and the diagnostic accuracy for malignant melanoma," *Exp. Dermatol.*, vol. 20, no. 8, pp. 648–652, Aug. 2011, doi: 10.1111/j.1600-0625.2011.01285.x.

[8] A. V. Mamishev, K. Sundara-Rajan, Fumin Yang, Yanqing Du, and M. Zahn, "Interdigital sensors and transducers," *Proc. IEEE*, vol. 92, no. 5, pp. 808–845, May 2004, doi: 10.1109/JPROC.2004.826603.

[9] X. Hu and W. Yang, "Planar capacitive sensors – designs and applications," *Sens. Rev.*, vol. 30, no. 1, pp. 24–39, Jan. 2010, doi: 10.1108/02602281011010772.

[10] J. Li, F. Rossignol, and J. Macdonald, "Inkjet printing for biosensor fabrication: combining chemistry and technology for advanced manufacturing," *Lab Chip*, vol. 15, no. 12, pp. 2538–2558, 2015, doi: 10.1039/C5LC00235D.

[11] NovaCentrix, "Metalon ® JS-A DEV ET0 10 Silver Inkjet Ink Safty Datasheet." 2022.

[12] X. B. Li, S. D. Larson, A. S. Zyuzin, and A. V. Mamishev, "Design principles for multichannel fringing electric field sensors," *IEEE Sens. J.*, vol. 6, no. 2, pp. 434–440, Apr. 2006, doi: 10.1109/JSEN.2006.870161.

[13] G. Schaumburg, "Novocontrol Introduces High Quality Low Cost Interdigitated Comb Electrodes," *Dielectr. Newsl.*, no. december, pp. 1–8, 2006.

[14] M. Ibrahim, J. Claudel, D. Kourtiche, and M. Nadi, "Geometric parameters optimization of planar interdigitated electrodes for bioimpedance spectroscopy," *J. Electr. Bioimpedance*, vol. 4, no. 1, pp. 13–22, Mar. 2013, doi: 10.5617/jeb.304.

[15] T. T. Ngo, H. Shirzadfar, D. Kourtiche, and M. Nadi, "A planar interdigital sensor for bio-impedance measurement: Theoretical analysis, optimization and simulation," *J. Nano- Electron. Phys.*, vol. 6, no. 1, pp. 1–7, 2014, [Online]. Available: https://essuir.sumdu.edu.ua/handle/123456789/35827.

[16] T. Barth, V. S. Teixeira, and W. Krautschneider, "Designing electrodes for electrical impedance spectroscopy in a four terminal setup," *Trans. Addit. Manuf. Meets Med.*, vol. 1, no. September, pp. 6–8, 2019, doi: 10.18416/AMMM.2019.1909S02T01.

[17] O. S. Andersen, "Cellular Electrolyte Metabolism," in *Encyclopedia of Metalloproteins*, R. H. Kretsinger, V. N. Uversky, and E. A. Permyakov, Eds. New York, NY: Springer New York, 2013, pp. 580–585.

[18] C. H. Hamann and W. Vielstich, *Elektrochemie*, 4. Weinheim: WILEY_VCH Verlag GmbH, 2005.